

## Guard ring design for high voltage operation of silicon detectors

Lars Evensen, Anders Hanneborg, Berit Sundby Avset and Martin Nese

SINTEF SI, P.O. Box 124 Blindern, N-0314 Oslo, Norway

Received 6 July 1993

The termination of the depletion zone towards the non-depleted part of silicon affects the total device leakage current, the long term stability, the noise level and the radiation hardness of silicon detectors. This paper describes computer simulations and experiments to develop guard ring structures for use in silicon detectors requiring thick depletion layers, high operating voltages and biasing beyond depletion without increase in the leakage current and the noise. Computer simulation of a simplified structure is used to understand the influence from the oxide charges and the substrate doping concentration for a segmented guard structure with several floating diffusion strips. Results from the simulations are compared with measurements on devices. The numerical results are found to be in agreement with experimental data. It is found that segmented guard structures with floating diffusion strips have high breakdown voltages and low leakage currents. The effects of floating metal field plates over the oxide between the floating diffusion strips are studied on two different guard structures by measuring the potential on the diffusion strips and the leakage currents in the guard and active diode. The results show that floating intermediate field plates reduces the influence from oxide charges and stabilises the device against environmental influence.

### 1. Introduction

Silicon detectors are used for detecting ionising radiation in high energy experiments. The detector systems planned for future machines like the Superconducting Supercollider (SSC) and the Large Hadron Collider (LHC), are larger than in any previous experiment. Silicon detectors will be used to a larger extent than before, they need to be more advanced and will operate at higher radiation levels than in earlier experiments. Thus more stringent requirements to radiation hardness are placed upon these future detectors.

The silicon detectors we consider are reverse biased p–n junction detectors passivated by thermally grown silicon dioxide. The application requires them to be operated at a high voltage to maximise the signal and reduce the charge collection time. Neutron radiation as expected in the SSC and LHC is known to change the depletion voltage of silicon detectors. The large volume of the detector systems will cause inhomogeneous radiation damage levels, thus increase the variation in depletion voltage among the detectors. The latter conditions either require each detector to operate at its own voltage or to be biased beyond depletion. Thus a guard ring design should pay special attention to high voltage operation.

One effect of the radiation on silicon devices comes from the build-up of permanent oxide charges in their SiO<sub>2</sub> layer. In radiation hardness experiments it has been observed that the oxide charges saturate at a level

of  $3 \times 10^{12} \text{ cm}^{-2}$  [1]. This level can be taken as an indication of the radiation induced oxide charge one should design detectors for since the oxide charge can have unwanted effects on devices. One of these is lowered breakdown voltages of p–n junctions when these terminate (in the plane of the p–n junction) on the Si/SiO<sub>2</sub> interface (see also fig. 1). In this paper we are mainly concerned with the effect of a guard ring to counteract the unwanted effects of the oxide charge. Generally a guard ring also serves other purposes as well. The main purpose of a guard ring is to reduce the dark current in the active area by decoupling the

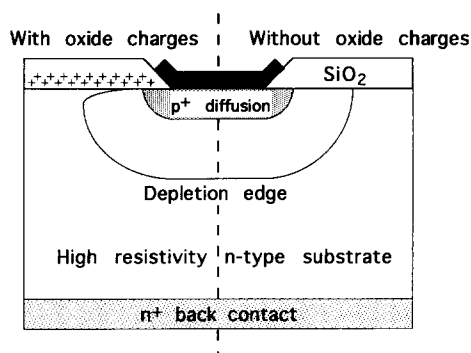


Fig. 1. Influence of oxide charges on a one-sided p–n junction in high resistivity silicon. A positive oxide charge gives a narrower depletion width along the surface than without oxide charges.

current generated outside the active area. The guard ring can also eliminate high field regions that otherwise could cause avalanche breakdown.

The present work was initiated by the requirements of a fast detector for electron spectroscopy up to 1 MeV that required a detector thickness of 1 mm to ensure total absorption of high energy electrons and positrons. The response time of the system should be less than 2 ns [2]. The detectors have to operate at a voltage higher than the depletion voltage without increase in the leakage current or noise. This could not be achieved with a conventional guard ring. To fulfill these requirements, a new guard ring structure was developed and results from this development are presented and discussed.

The influence from charges in the oxide and on top of the oxide on the guard ring design is considered in section 2 together with different design concepts. The guard ring structures used in our experiments and simulations are described in section 3. We are in this paper mainly interested in the spatial distribution of the electric potential and we present experimental and calculated results of this in section 4. The results are discussed in section 5 while a summary with conclusions are made in section 6.

## 2. Guard design considerations

A net positive oxide charge causes accumulation of electrons along the silicon surface for n-type doping and depletion of holes along the surface for p-type doping. For a one-sided step junction in high resistivity n-type silicon, this accumulation layer will give a narrower depletion region along the surface compared to the situation in the planar bulk area or if oxide charges were not present. A comparison of the situation with and without oxide charges is shown in fig. 1. The oxide charges, which are assumed independent of the bulk doping density, will influence the width of the depletion region more in high resistivity silicon than they will in low resistivity silicon. With a constant potential difference across the depletion region, reduction of the

depletion width will increase the field in the silicon close to the interface between silicon and silicon dioxide. Consequently, avalanche breakdown is more likely to occur in the surface region of high resistivity substrates than in low resistivity substrates and surface avalanche breakdown is also considered the most common breakdown mechanism of standard silicon detectors that are usually made from high resistivity silicon.

The chemical stability of the silicon dioxide surface depends very much on the final processing conditions. The surface of the oxide is usually hydrophilic and the charge density and conductivity can be altered by changes in the environmental conditions [3,4]. The silicon dioxide surface should be considered as chemically and electrically unstable. As pointed out by Longoni et al. [4] this may be one of the main reasons for instabilities in silicon detectors having an insufficient environmental passivation compared to a packaged integrated circuit. Although the bulk oxide charges generally are considered to be positive, additional negative charges on the oxide surface can give a net negative oxide charge that will invert n-type silicon. Positive charges on the oxide surface in addition to the bulk charges, will reduce the depletion width in the silicon more than the bulk oxide charges alone and thereby reduce the avalanche breakdown voltage. Large unpassivated silicon dioxide surfaces around biased p-n junctions should be avoided. Injection of high energy electrons into the oxide from high field regions in the silicon can also alter the net oxide charge and change the charge state of floating electrodes.

Much work has been carried out to improve and optimise the design and performance of power devices where guard ring structures have been shown necessary for high voltage operation. Three different approaches are generally used to control the termination of the depletion region. The simplest approach is to include metal field plates on top of the oxide outside the junction [5,6] to eliminate variation in the charge on the oxide surface and reduce the influence from bulk oxide charges. Variation in the lateral doping density by implantation has also been used [7]. This method requires several masking procedures and does not avoid

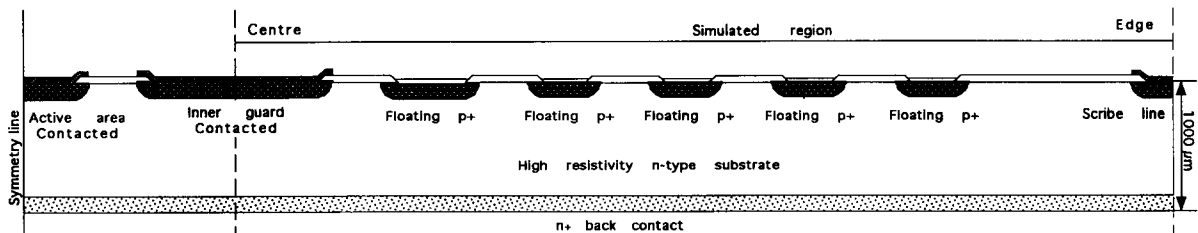


Fig. 2. Detailed drawing of the experimental guard structure. The substrate thickness is 1000  $\mu\text{m}$ . Only that part indicated was simulated.

the influence from variations in the net oxide charge. The third method, which we have investigated, is to surround the centre diode with one or several p–n junctions that are not contacted or biased [8,9].

We have studied a guard ring structure with several floating  $p^+$  diffusions in high resistivity n-type silicon both by computer simulation and by experiment. We have named the structure shown in fig. 2 a multiguard. Bias is applied to the  $n^+$  back contact, the active area and the inner guard are grounded. The essential mechanism of the guard is as follows. When the bias is increased, the depletion region extends around the inner contacted guard ring. At a certain bias the first non-contacted  $p^+$  diffusion will charge up. This situation is known as punchthrough. The punchthrough voltage depends on the bulk doping concentration, the distance between the two  $p^+$  diffusions and on the net oxide charge. The maximum field strength for a given doping concentration and oxide charge is, to first order (low dark current), controlled by the distance between the two  $p^+$  diffusions. Further increase in the bias voltage will give a fractional increase in the potential on the first non-contacted  $p^+$  diffusion while the depletion region extends around the two  $p^+$  diffusions. The same procedure is repeated for the other floating strips. This will distribute the potential outside the centre contacted diode over a larger distance and give a lower maximum field strength compared to the situation for a single p–n junction. The detector can therefore be biased at a higher voltage before avalanche breakdown is observed. While the potential distribution along the Si/SiO<sub>2</sub> interface can easily be predicted qualitatively, simulations are needed to make quantitative predictions as will be described later.

We have also incorporated metal field plates between the diffused  $p^+$  guard rings on processed devices. In addition to this structure, we have investigated the effect of varying geometries on two differently processed devices. The metal field plates are in all cases left floating and will acquire a potential that depends on the conductivity to the closest defined potentials.

### 3. Experimental details and simulation model

We have designed 1 cm × 1 cm square diodes surrounded by a guard structure as shown in fig. 2. The gaps between  $p^+$  diffusions were 50 μm and the width 25 and 50 μm. The guard strips with rounded corners were covered by oxide except for small metal pads used for probing the guard potential. All devices were processed on high resistivity silicon with diffused p and n regions. The wafers were approximately 1000 μm thick and bias was applied between the front side diodes and the back side ohmic contact.

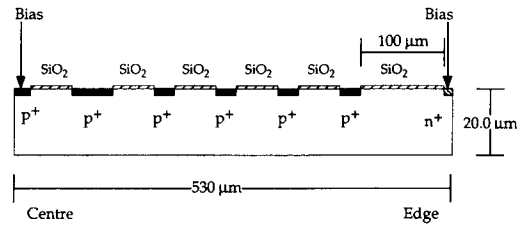


Fig. 3. Simplified structure used in the simulations. The gaps are 50 μm and the strips are 25 or 50 μm.

To reveal the essential features of the experimental structure described above, we have modelled it by the simplified structure shown in fig. 3 for the simulations. Bias was applied laterally between the centre guard ring diode and the  $n^+$  ohmic contact in the surface. The simulated guard structure was 20 μm thick to reduce the number of grid points and focus on the region where the oxide charges influences the potential distribution. The potential imposed on the  $n^+$  contact is not necessarily the same as that applied on the backside. This contact will go through the potentials we have simulated when bias is applied on the back contact and the potential difference between the two contacts will be small if the leakage current is small.

We used computer simulations to predict the behaviour of the guard structure with different substrate doping concentrations and under the influence from oxide charges. We simulated the simplified structure shown in fig. 3 with the general purpose 2D device simulator PISCES-2B [10], that solves both the Poisson and continuity equations for holes and electrons. The effect of floating metal field plates is not studied by simulation. Dirichlet boundary conditions are imposed in the ohmic contacts where surface potential, electron and hole concentrations are fixed. Homogeneous (reflecting) Neumann boundary conditions are imposed along the outer non-contacted edges of the device. In the absence of surface charge along such edges, the normal electric field component becomes zero. Current is not allowed to flow into isolating regions. The boundary conditions on the outer oxide surface is imposed indirectly by specifying the boundary conditions in the interface between silicon and oxide. Oxide charges are assumed along this interface. Two carrier solutions were made assuming Shockley–Read–Hall generation and recombination, Auger recombination, impact ionisation and concentration and field dependent mobilities.

Substrate doping concentrations used in the simulations were chosen to be close to experimental ones. The concentration thus determined were  $4.3 \times 10^{11}$  atoms/cm<sup>3</sup> for wafers with a resistivity of 8 kΩ cm and  $2.1 \times 10^{11}$  atoms/cm<sup>3</sup> for wafers with a resistivity greater 10 kΩ cm. These doping concentrations were

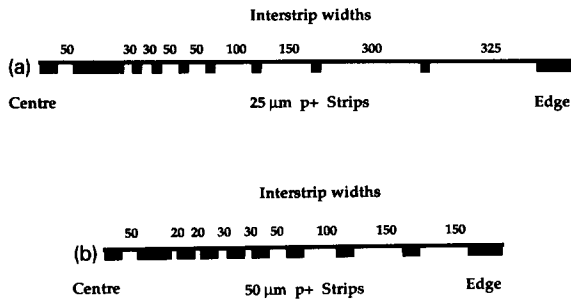


Fig. 4. Design of the guard structures used to study the influence from floating metal field plates by measuring the individual strip potentials. The metal field plates are not shown for clarity. Dimensions are listed in table 1.

calculated from the depletion voltage extracted from  $C-V$  measurements on the experimental diodes. In addition, one case assumed a doping concentration of  $1.5 \times 10^{12}$  atoms/cm<sup>3</sup>, equivalent to a resistivity of 3 kΩ cm. All implants were considered to have a Gaussian impurity profile and three different oxide charge levels,  $Q_f = 1 \times 10^{10}$  cm<sup>-2</sup>,  $Q_f = 8 \times 10^{10}$  cm<sup>-2</sup>, and  $Q_f = 3 \times 10^{11}$  cm<sup>-2</sup>, were simulated.

Test samples with the guard ring design shown in fig. 2 were made on n-type wafers with (111) orientation and 1 mm thickness. The resistivity of the wafers was either 8 kΩ cm or greater than 10 kΩ cm. A description of the process is given in ref. [2].

Test samples were also processed on n-type, 5 kΩ cm silicon wafers of 380 μm thickness and a (100) orientation to study the effect of floating metal field plates. The process was identical to the one mentioned above and the samples are marked as T16-Oct91-2. The guard ring designs shown in figs. 4a and 4b were used together with either wide or narrow floating metal field plates between guard strips. The narrow field plate width was 7.5 μm for the smallest gap distances and 17.5 μm for the wider gaps. Wide field plates were designed to be 10 μm narrower than the gap between guard strips. However, the narrow and wide field plates have the same width when the gaps between diffusion strips are less than 50 μm. A compilation of the field plate data is given in table 1.

All samples were visually inspected for defects to exclude samples with shorts between the diffusions. Bias was applied to the ohmic backside contact with a Keithley 487 Voltage source while grounding the active diode and the innermost wide guard strip. The potential distributions among the strips were measured by connecting a Keithley 617 Electrometer between the innermost guard ring and the floating strip to be measured. Leakage currents were measured with a Keith-

Table 1

Dimensions for the field plates and gaps of Test structure 1 and 2. All dimensions are measured in μm

Test structure 1			Test structure 2		
Gap width	Wide field plate	Narrow field plate	Gap width	Wide field plate	Narrow field plate
30	7.5	7.5	20	7.5	7.5
30	7.5	7.5	20	7.5	7.5
50	30	17.5	30	7.5	7.5
50	30	17.5	30	7.5	7.5
100	80	17.5	50	30	17.5
150	130	17.5	100	80	17.5
300	280	17.5	150	130	17.5
325	305	17.5	150	130	17.5

ley 617 Electrometer in the current mode and two Keithley 487 Picoammeters.

## 4. Results

### 4.1. Simulations

The potential along the surface of a plain diode similar to that shown in fig. 1 with a bulk doping concentration of  $5.6 \times 10^{11}$  cm<sup>-3</sup> are shown in fig. 5. The potential on the n<sup>+</sup> contact was assumed to be 100 V and it was assumed evenly distributed oxide charge densities of 0 cm<sup>-2</sup>,  $8 \times 10^{10}$  and  $3 \times 10^{11}$  cm<sup>-2</sup> in the interface between silicon and silicon dioxide. It can be seen that the potential and thereby the depletion width

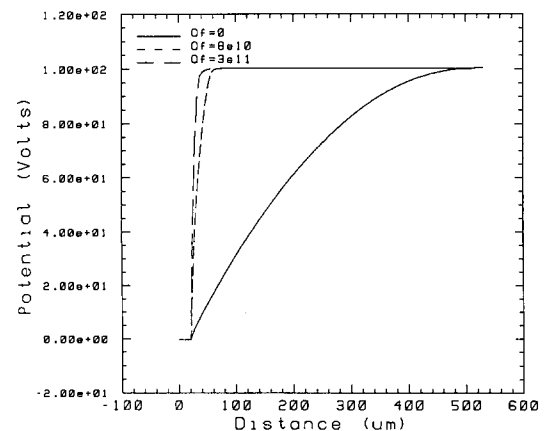


Fig. 5. Results from simulation of the potential distribution along the surface for a reverse biased step junction as shown in fig. 1 assuming three different oxide charge densities. The doping concentration was  $5.6 \times 10^{11}$  atoms/cm<sup>3</sup>. The leftmost curve is for an oxide charge of  $3 \times 10^{11}$  atoms/cm<sup>3</sup>, the middle curve is for an oxide charge of  $8 \times 10^{10}$  atoms/cm<sup>3</sup> while the right curve is without oxide charge. The bias was 100 V.

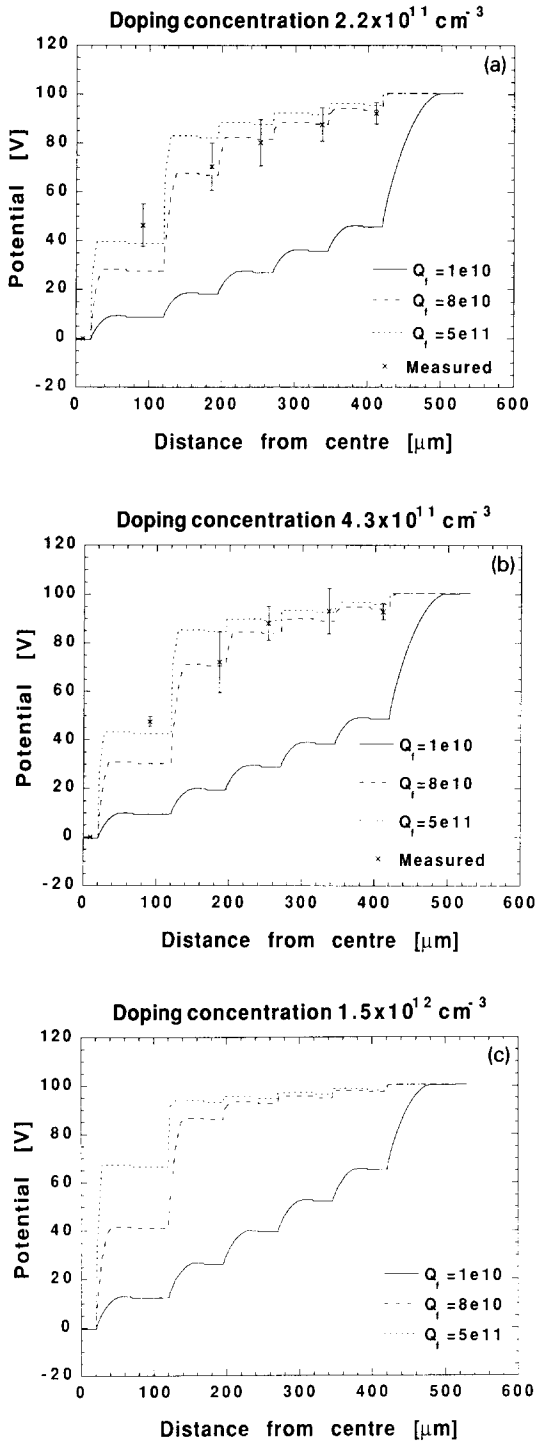


Fig. 6. Results from simulation of the potential distribution along the surface for the guard ring structure shown in fig. 3. The three plots show results for the same geometrical structure with different oxide charge densities and substrate doping concentrations. Measurements on real devices are plotted ( $\times$ ) for comparison. The error bars are the variance for measurements on at least three identical structures.

along the surface of diodes passivated with silicon dioxide varies considerably with oxide charge density. The applied bias is distributed over 500  $\mu\text{m}$  if the oxide charge is assumed to be zero, while for the highest oxide charge density, the applied bias is dropped over a distance of 40  $\mu\text{m}$ . The maximum field strength will also vary considerably because of the difference in potential distribution.

The structure shown in fig. 3 was used to study the influence from bulk doping concentration and oxide charge density on the potential distribution in a segmented guard structure. The results are shown in fig. 6 for a bias of 100 V. It is seen that for the low oxide charge density there is an almost equal potential difference between all the adjacent  $p^+$  diffusions while the potential difference between the outermost  $p^+$  diffusion and the  $n^+$  contact is larger. The potential difference between adjacent strips increases with increasing doping concentration and increasing oxide charge. Both the position and magnitude of the maximum potential difference between strips can be seen to depend on substrate resistivity as well as oxide charge. The general behaviour is that an increase in the oxide charge moves the main potential drop towards the centre strips while a low oxide charge gives a large potential drop between the outer strip and the  $n^+$  contact.

#### 4.2. Electrical measurements

Measurements of the individual strip potentials on samples with 1 mm thickness and the guard design shown in figs. 2 are also plotted in fig. 6a and 6b. Measurements and simulations can be compared in fig. 6a for substrates with an estimated doping concentration of  $2.2 \times 10^{11}$  atoms/ $\text{cm}^3$ . Fig. 6b shows potential measurements and simulations for an estimated doping concentration of  $4.3 \times 10^{11}$  atoms/ $\text{cm}^3$ . To compare measurement and simulation one should use the data for an oxide charge of  $8 \times 10^{10} \text{ cm}^{-2}$ . This oxide charge density is estimated from  $C-V$  measurements on MOS capacitors processed with an identical process. The measurements follow the general behaviour of the simulations except for some discrepancy for the strips close to the centre. The error bars are the standard deviation of measurement on at least three identical structures. There are rather large relative variations found on identically processed structures.

The guard designs in fig. 4 were used to study the effect of metal field plates between the floating diffusion strips and the results are shown in fig. 7. Crosses represent the measurements while the lines are drawn to guide the eye. The potentials of individual guard strips were measured with bias applied to the back contact and varied in 50 V increments. The active area and the centre guard contact were grounded. All the measurements identified with T16-Oct91-2 and re-

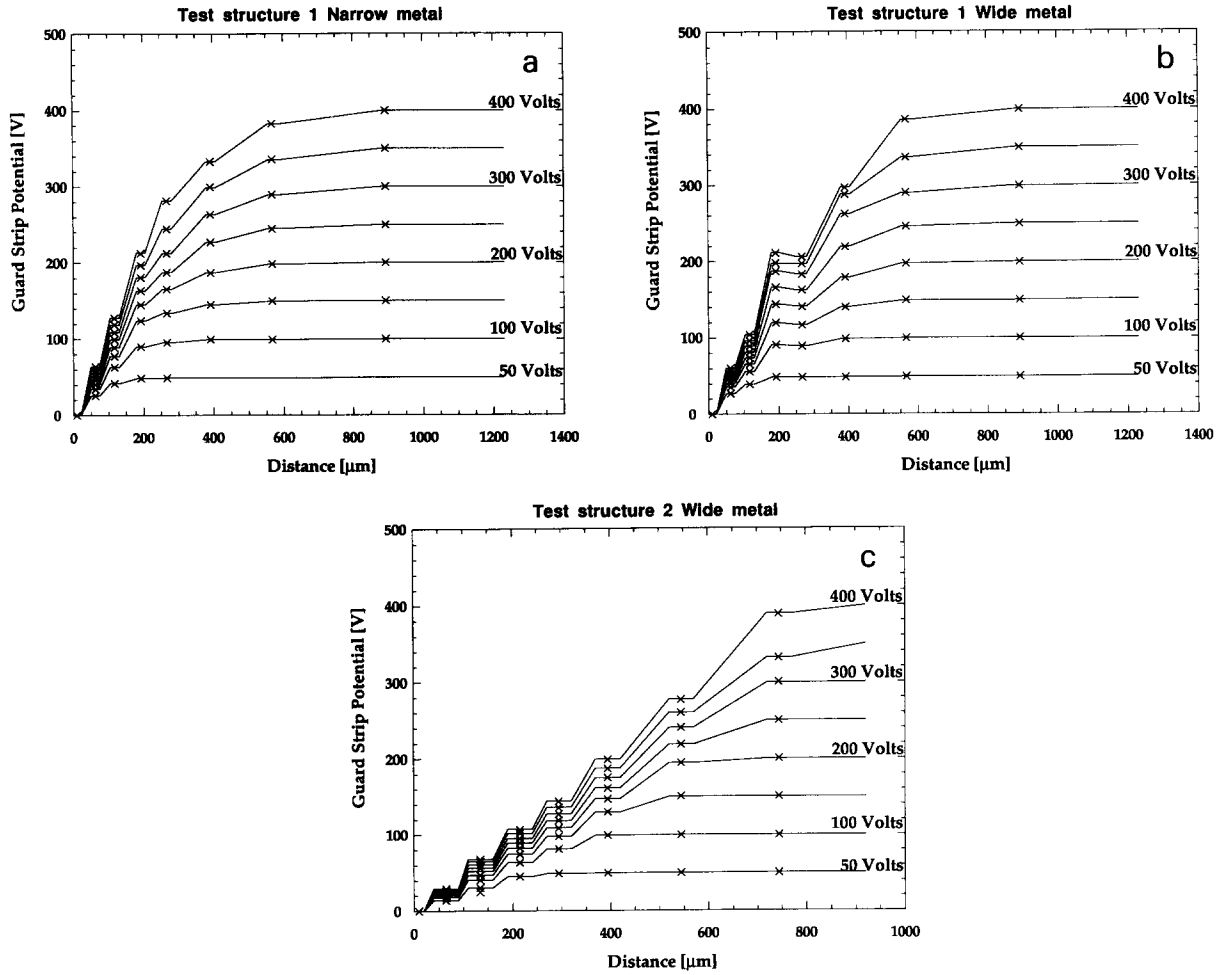


Fig. 7. Measurements of the individual guard strip potentials on the multiguard structures shown in fig. 4 with floating interstrip metal field plates. The lines are drawn to guide the eye while the crosses ( $\times$ ) represent the measurement.

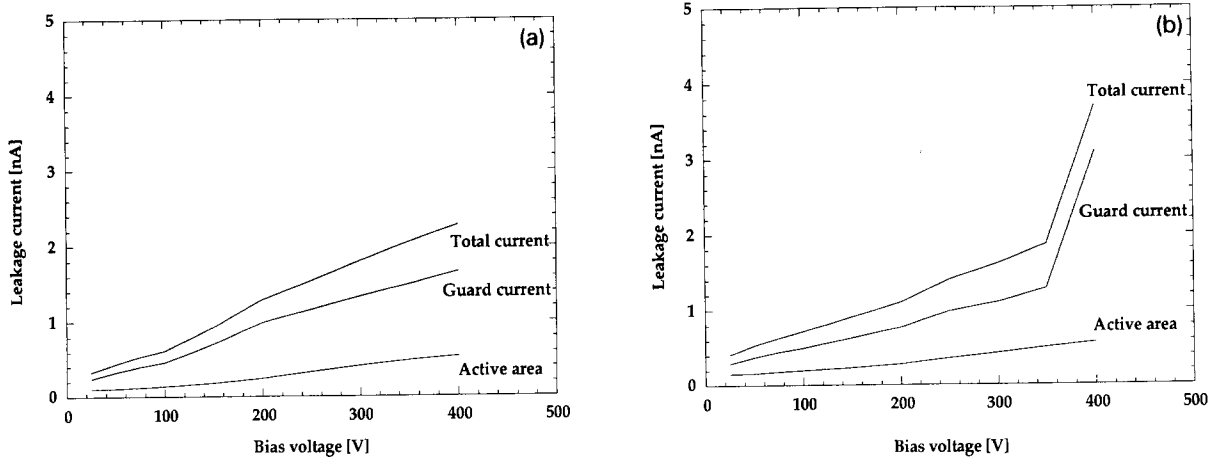


Fig. 8. Leakage current measurements on (a) Test structure 1 with wide field plates and (b) Test structure 2 with narrow field plates. The guard ring design is shown in fig. 4.

ferred to in the next paragraphs are from the same wafer to minimise effects from variations in the oxide charge density.

Fig. 7 shows measurement of the guard strip potentials at different biases. It can be seen that more strips float to a potential that differs significantly from the applied bias as the voltage on the back side is increased. The potential on the centre strip is only a fraction of the applied bias and its potential increases only weakly with increasing bias and never reaches the full bias value. The outer guard strips have a potential that deviates little from the applied bias voltage.

Fig. 7a shows potential measurements on Test structure 1 with wide gaps and narrow field plates and fig. 7b shows potential measurements on Test structure 1 with wide gaps and wide field plates. Most of the potential difference is between the inner guard strips where the potential increases fast with the bias voltage. No significant difference can be seen between wide and narrow field plates when figs. 7a and 7b are compared. Fig. 7c shows potential measurements on Test structure 2 with narrow gaps and wide metal field plates. The potential distribution between adjacent floating guard strips of Test structure 2 is almost uniform and several guard strips have a potential that differs from the applied bias value even at the lowest applied bias. The potential on the centre guard strip increases less with bias compared to that for the cases in figs. 7a and 7b. The potentials on the centre floating guard strip is also much lower for Test structure 2 than for Test structure 1. A significant difference can be seen in the potential distribution when fig. 7b with wide gaps and fig. 7c with narrow gaps are compared. Wide metal field plates are applied in both cases.

The leakage currents in the guard and in the active area of  $1\text{ cm} \times 1\text{ cm}$  diodes, are shown in fig. 8. The measurements were made on the same structures as shown in figs. 7a and 7c. The  $380\text{ }\mu\text{m}$  of silicon is depleted at  $90\text{ V}$  and the room temperature active area leakage current is  $600\text{ pA}$  at an applied bias of  $400\text{ V}$ . Test structure 1 with the wide gaps and narrow metal field plates (fig. 8a) has no increase in current up to  $400\text{ V}$ . The leakage current in the guard of Test structure 2 with the narrow gaps and wide metal field plates (fig. 8b) increases between  $350$  and  $400\text{ V}$  without any associated increase in the active area current.

## 5. Discussion

We have designed a guard structure with several floating p-n junctions by considering the potential distributing effect a part of its essential functions. We have used computer simulations of a model of this structure to study the potential distribution in the structure for different doping concentrations and oxide

charge densities. We have made potential measurements at the guards of experimental samples to investigate the correctness of the simulated model and improve our understanding of real devices. The topics to be discussed in this section are interwoven in each other and we will first comment and discuss the general validity of the computer simulations. Then we discuss the effect of metal field plates in the guard design. Metal field plates were not incorporated in simulations. Finally we discuss the general behaviour and tendencies we have simulated and measured. We will also indicate how the results best can be utilised in future design of optimised guard structures.

The key factors determining the potential and the maximum field strength in the multiguard structures are the lowest doping concentration, the oxide charge density and the distance between guard strips. The  $p^+$  diffusions have constant potentials and will not influence the breakdown behaviour. We find the potential distributions we simulate on multiguard structures to be at least qualitatively in agreement with our intuitive expectations. We take this as an indication that the simulated model gives results that are qualitatively correct and yield potential values that are close to correct values for the idealised situations the model structures were supposed to represent. Experimentally observed tendencies are easier to explain if correctness of the simulations is assumed rather than explanations according to intuitive expectations. The latter, at least for this discussion, tends to yield long arguments.

The above arguments make it important to find out whether the experimentally measured potential distributions are dependent upon factors we have considered in the simulations. If other factors dominated the behaviour, we would have to include them if their values could be predicted.

Otherwise, we should ideally eliminate them. Figs. 6a and 6b can be used as an example where the bulk doping concentration is deliberately different. For an oxide charge around  $8 \times 10^{10}\text{ cm}^{-2}$  we expect from simulations that the potential on the first strips from the centre to increase when the substrate doping is increased (also shown in fig. 6). The size of the standard deviations seen in the measurements indicates that in order to test any tendencies critically they have to yield relatively large theoretical effects. However, the expected differences are smaller than the standard deviations shown for the measurements. Thus the measured variation of potential with doping concentration agrees with the simulations.

If we consider the general shape of the measured potential distributions in figs. 6a and 6b we notice that they resemble the simulated ones when an oxide charge around  $8 \times 10^{10}\text{ cm}^{-2}$  is assumed. There is perhaps a tendency for the first strip from the centre to have a mean measured potential that is higher than simulated.

Considering the limited statistics and the size of the typical standard deviation for the measurements it is not clear that there is a systematic deviation. It is clearly a too weak tendency to justify a re-evaluation of the simulations. Still we think further work should be done to evaluate how the simulated potentials depend upon input parameters such as bulk generation rates and depth of the  $p^+$  strips, which are factors we believe could influence the potential on the guard strips in the presence of oxide charges. It will also be important to simulate the full guard structure if the bulk generation rate is critical for the potential distribution.

We will now describe the physical effect of the floating metal plates in the guard designs. Metal on top of the oxide will eliminate variations in the charge on the oxide due to environmental changes. Additionally, the high electron concentration of the outer metal surface will reduce the influence from changes in the environmental conditions (including charges external to the metal) on the charge concentrations in the silicon surface. Without metal field plates on top of the oxide most of the oxide charge is mirror imaged in the underlying silicon. Floating metal field plates will reduce the effect from oxide charges by providing image charges in the metal. This effect will depend both on the location of the charges in the oxide and on the oxide thickness. From the above argument, we predict that the presence of the metal field plate will act similarly to reducing the oxide charge for n-type material with an oxide charge that is normally positive. This justifies comparisons between experiments having field plates and simulations having no field plates, as long as the obvious cautions are kept in mind.

From the above we expect that increasing the width of the field plates in our guard structures will act similarly to reducing the oxide charge. Thus the depletion width along the surface will increase. In principle, one could observe this effect in structures with different floating metal field plate widths. Figs. 7a and 7b show Test structure 1 for narrow and wide field plates respectively. The effects, if any, of the metal plate widths are not observable here. First, as mentioned in section 3 and shown in table 1, it should be noticed that the widths are different only from the third plate and outwards, thus not for the innermost ones. From the simulations we expect the innermost strips to have the strongest dependence of potential variations on oxide charge. We also notice that the irregular potential distribution seen in fig. 7b may conceal the effects from an increase in field plate width. Clearly, arbitrary variations are still larger than the effects of metal field plates on the oxide charge, if any. These arbitrary variations include effects such as variation in oxide charge, localised surface and bulk defects and charges from the environment on uncovered oxide regions. A

metal plate still should have the beneficial protecting effect as described and we believe this to be a good reason to keep them in the design. The presence of the metal plate can also be active in distributing the potential as considered in the following.

Inclusion of metal field plates changes the guard structure and the potential distribution between  $p^+$  diffusions depending on the MOS threshold voltage, the field plate potential and the silicon surface potential distribution. The potential on the floating field plates will depend on the conductivity of the oxide surface and on the bulk resistivity of additional passivation coatings. The conductivity on the oxide depends strongly on the environmental humidity [3] and the sheet resistance can be about  $10^{18}$   $\Omega$ /square at 40% relative humidity. The surface sheet resistance will influence the time constant for charging of the metal field plate. Operation of a multiguard can be improved by controlling the potential on the metal field plates either by connecting them directly to defined potentials by a resistor network or by connection to the floating p-n junction.

By decreasing the distances between the guard strips, the potential difference between strips will decrease, more of the surface will be depleted at a given bias voltage and the potential drop will be distributed across a larger distance along the surface. This can be seen by comparing fig. 7b (wide gaps) with fig. 7c (narrow gaps). Wide field plates are used in both cases and it can be seen from fig. 7c that the potential difference between guard rings can be limited and well controlled by applying small gaps and wide field plates.

The difference in potential distribution will influence the leakage current at high bias as can be understood by considering the individual strip potentials and potential distributions in figs. 7a and 7c. It can be seen that the edge strip of Test structure 2 start to deviate from the applied bias voltage implying that the depletion region extends beyond this strip. This is accompanied by an increase in the leakage current above 350 V in fig. 8b. We speculate that the increase in guard current may be caused by an increased generation rate as the depletion region extends towards the edge. Another explanation, also yielding increased current, assumes localised high field regions in the device that causes avalanche breakdown. If that had been the case we would expect the current to increase dramatically with bias. However, we observe that a 50 V increase in bias voltage only causes the guard current to double. So we think it is more likely that the depletion region extends to the edge where crystal damage causes the leakage current to increase.

The results of the simulations shown in fig. 6 indicate that the potential difference between strips will be almost equal at a very low oxide charge density and the depletion region will reach the edge of the detector.

This guard design should give a high breakdown voltage with an increase in the leakage current as the depletion region extends out to the edge. Using a wider guard region and include more guard strips should solve the problem of the depletion region extending to the edge. The distance between the centre guard strips should be reduced to avoid large potential differences and an increased probability for avalanche breakdown.

For operation in a radiation environment the total dose and oxide charge should be considered during design of the guard structure and sufficient space allowed for an optimum guard structure. The minimum guard width will be the depletion width at the operating voltage plus the width of all p-n junctions beyond the centre biased one. The net positive oxide charge can reduce this width by imposing a higher electron concentration along the surface. However, operation in a radiation environment will change the oxide charge with time thus change the optimum guard design. Increasing the doping concentration by implantation of phosphorous can be used to reduce the total guard width in a controlled manner. The use of floating metal field plates will reduce the effect of the oxide charge and increase the minimum guard width towards the depletion width at the operating voltage. Metal field plates connected to the floating p<sup>+</sup> diffusions will increase or decrease the potential difference between strips depending on if they extend towards the higher or lower potential side of the strip they are connected to. This work will also be important for the understanding, design and operation of silicon drift chamber devices [11] and silicon microstrip detectors [12].

## 6. Summary and conclusions

We have simulated the potential distribution and tested the performance of a segmented guard structure with floating p<sup>+</sup> diffusion strips. The effect of floating metal field plates between the floating p<sup>+</sup> junctions has been investigated experimentally. It is shown that such structures can be used to control (to some degree) the termination of the depletion region along the surface by extending the depletion region. The effect of floating field plates between the guard strips is to reduce the influence from oxide charges and in addition reduce the environmental influence on the silicon dioxide surface charge. Segmented guard ring struc-

tures with floating metal field plates can give a low leakage current in the guard region at very high bias voltages.

To design an optimum multiguard structure the bulk doping concentration, the oxide charges and the operating voltage must be considered when deciding the interstrip gaps, the field plate widths, the number of guard rings and the total guard ring width. Simulations similar to those presented here will be valuable in the design of optimised structures.

## Acknowledgements

Special thanks to Professor Terje G. Finstad from the Department of Physics, University of Oslo for helpful discussion while writing this paper. This work has been supported in part by The Royal Norwegian Council for Scientific and Industrial Research (NTNF).

## References

- [1] D.D. Pitzl, N. Cartiglia, B. Hubbard, J. Leslie, K. O'Shaughnessy, W. Rowe, H.F. Sadrozinski, E. Spencer, H.J. Ziocck, P. Ferguson, E.C. Milner and W.F. Sommer, Nucl. Phys. B (Proc. Suppl.) 23A (1991) 340.
- [2] L. Evensen, A. Hanneborg, T. Happ, A.H. Wuosmaa and R.R. Betts, Nucl. Instr. and Meth. A 326 (1993) 136.
- [3] A.S. Grove, Physics and Technology of Semiconductor Devices, (Wiley, 1967).
- [4] A. Longoni, M. Sampietro and L. Strüder, Nucl. Instr. and Meth. A 288 (1990) 35.
- [5] C.B. Goud and K.N. Bhat, IEEE Trans. Electron Devices ED-38 (1991) 1497.
- [6] D. Jaume, G. Charitat, J.M. Reynes and P. Rossel, IEEE Trans. Electron Devices ED-38 (1991) 1681.
- [7] R. Stengl, U. Gösele, C. Fellingner, M. Beyer and S. Walesch, IEEE Trans. Electron Devices ED-33 (1986) 426.
- [8] B.J. Beluga, Solid-State Electron. 33 (1990) 485.
- [9] K.-P. Brieger, W. Gerlach and J. Pelka, Solid-State Electron. 26 (1983) 739.
- [10] M.R. Pinto, S.R. Connor and R.W. Dutton, PISCES2 – Poisson and Continuity Equation Solver, Stanford Electronics Laboratory Technical Report, Stanford University, 1984.
- [11] B.S. Avset, L. Evensen, G. Hall, S. Roe and R. Wheadon, Nucl. Instr. and Meth. A 310 (1991) 203.
- [12] B.S. Avset et al., IEEE Trans. Nucl. Sci. NS-37 (1990) 1153.